

THE CARNEGIE-CHICAGO HUBBLE PROGRAM. V. THE DISTANCES TO NGC 1448 AND NGC 1316
VIA THE TIP OF THE RED GIANT BRANCH*

DYLAN HATT,¹ WENDY L. FREEDMAN,¹ BARRY F. MADORE,^{1,2} IN SUNG JANG,³ RACHAEL L. BEATON,^{4,†}
TAYLOR J. HOYT,¹ MYUNG GYOON LEE,⁵ ANDREW J. MONSON,⁶ JEFFREY A. RICH,² VICTORIA SCOWCROFT,⁷ AND
MARK SEIBERT²

¹*Department of Astronomy & Astrophysics, University of Chicago, 5640 South Ellis Avenue, Chicago, IL 60637*

²*Observatories of the Carnegie Institution for Science 813 Santa Barbara St., Pasadena, CA 91101*

³*Leibniz-Institut für Astrophysik Potsdam, D-14482 Potsdam, Germany*

⁴*Department of Astrophysical Sciences, Princeton University, 4 Ivy Lane, Princeton, NJ 08544*

⁵*Department of Physics & Astronomy, Seoul National University, Gwanak-gu, Seoul 151-742, Korea*

⁶*Department of Astronomy & Astrophysics, Pennsylvania State University, 525 Davey Lab, University Park, PA 16802*

⁷*Department of Physics, University of Bath, Claverton Down, Bath, BA2 7AY, United Kingdom*

ABSTRACT

The *Carnegie-Chicago Hubble Program* (CCHP) is re-calibrating the extragalactic SN Ia distance scale using exclusively Population II stars. This effort focuses on the Tip of the Red Giant Branch (TRGB) method, whose systematics are entirely independent of the Population I Cepheid-based determinations that have long served as calibrators for the SN Ia distance scale. We present deep *Hubble Space Telescope* imaging of the low surface-density and low line-of-sight reddening halos of two galaxies, NGC 1448 and NGC 1316, each of which have been hosts to recent SN Ia events. Provisionally anchoring the TRGB zero-point to the geometric distance to the Large Magellanic Cloud derived from detached eclipsing binaries, we measure extinction-corrected distance moduli of $31.23 \pm 0.04_{stat} \pm 0.06_{sys}$ mag for NGC 1448 and $31.37 \pm 0.04_{stat} \pm 0.06_{sys}$ mag for NGC 1316, respectively, giving metric distances of $17.7 \pm 0.3_{stat} \pm 0.5_{sys}$ Mpc, and $18.8 \pm 0.3_{stat} \pm 0.5_{sys}$ Mpc. We find agreement between our result and the available Cepheid distance for NGC 1448; for NGC 1316, where there are relatively few published distances based on direct measurements, we find that our result is consistent with the published SN Ia distances whose absolute scales are set from other locally-determined methods such as Cepheids. For NGC 1448 and NGC 1316, our distances are some of the most precise (and systematically accurate) measurements with errors at 1.7 (2.8) % and 1.6 (2.7) % levels, respectively.

Keywords: stars: Population II, cosmology: distance scale, galaxies: individual: NGC 1448, galaxies:
individual: NGC 1316

dhatt@uchicago.edu

* Based on observations made with the NASA/ESA *Hubble Space Telescope*, obtained at the Space Telescope Science Institute, which is operated by the Association of Universities for Research in Astronomy, Inc., under NASA contract NAS 5-26555. These observations are associated with program #13691.

† Hubble Fellow

Carnegie-Princeton Fellow

1. INTRODUCTION

The tension in the value of H_0 as determined by astrophysical methods (for a review and recent updates see [Freedman et al. 2012](#); [Riess et al. 2018](#)) and indirect/modeling methods (via the Cosmic Microwave Background; e.g. [Komatsu et al. 2011](#); [Planck Collaboration et al. 2018](#)) currently stands at $3.6\text{-}\sigma$. Uncertainties and possible unknowns in the systematics of the Cepheid-based distance scale, such as the metallicity dependence of the period-luminosity zero-point (e.g., [Sakai et al. 2004](#); [Klagyivik et al. 2013](#); [Mager et al. 2013](#)) and the pervasiveness of source blending in extragalactic studies ([Mochajska et al. 2004](#); [Vilardell et al. 2007](#)), have motivated the *Carnegie-Chicago Hubble Program (CCHP)*, which aims to re-calibrate the SN Ia extragalactic distance scale using an independent path based on Population (Pop) II stars (a summary of the program is given in [Beaton et al. 2016](#), Paper I). Since distances derived from Pop II stars are completely decoupled from the systematics encountered in the Pop I path, they can provide insight into the current divide in the measurement of H_0 .

Pop II stars are a natural—and in most cases, the preferred—substitute for Pop I stars as distance indicators. Unlike Pop I stars, which are typically found in the crowded and dusty disks of spiral and irregular galaxies, Pop II stars can be universally found in the uncrowded, metal-poor, and virtually dust/gas-free outer halos of all galaxy types. The Pop II stars of focus for the CCHP are low-mass Red Giant Branch (RGB) stars at the end of the giant-branch evolutionary phase. These stars experience a rapid lifting of core-degeneracy, culminating in the He-flash and evolution into stable He-core burning at lower luminosities and bluer colors along the zero-age Horizontal Branch. This abrupt transition is sparked by a critical core mass that is weakly dependent on core metallicity and total star mass ([Salaris & Cassisi 2005](#)). Consequently, the tip of the RGB (TRGB) is a sharply-defined feature in Color-Magnitude Diagrams (CMDs), especially those of galaxy halos where few other stellar populations are present.

This paper is a continuation in a series that presents TRGB distances to nine nearby galaxies containing a cumulative 12 SN Ia. Previously we have published a distance to the Local Group galaxy IC 1613 ([Hatt et al. 2017](#), Paper II), which, although it does not have a SN Ia on record, is an invaluable calibrator for the TRGB distance scale. We have furthered measured a distance to NGC 1365 ([Jang et al. 2018](#), Paper III), host to SN 2012fr, as well as distances to NGC 4424, NGC 4526, and NGC 4536 ([Hatt et al. 2018](#), Paper IV), which are host to SN 2012cg, SN 1994D, and SN 1981B,

respectively. The distances to IC 1613 and NGC 1365 represent the extremes in distances for galaxies studied in the CCHP, approximately 730 kpc and 18.1 Mpc, which were measured to comparable precision owing to careful choice of field placement and the power of the TRGB method.

In this work we present TRGB distances to a further two SN Ia host galaxies, NGC 1448 and NGC 1316, using deep *Hubble Space Telescope (HST)* imaging of their halos. NGC 1448 is an edge-on spiral galaxy that is host to the SN Ia event SN 2001el ([Monard et al. 2001](#)), and NGC 1316 is a lenticular galaxy in the Fornax Cluster that is host to the two SN Ia events SN 2006dd and SN 2006mr ([Monard 2006](#); [Phillips et al. 2006](#)). These galaxies are believed to be comparable in distance to that of NGC 1365, which makes them extremely valuable test cases for the most distant TRGBs in the CCHP sample.

The paper is organized as follows: Section 2 describes the observations and photometry; Section 3 presents the analysis of the TRGBs, including the estimation of measurement uncertainties and the determination of distances; Section 4 places the distances measured here in context with previously-published estimates, including a Cepheid-based determination for NGC 1448; and Section 5 provides a summary and the immediate impact of the results presented in this study.

2. DATA

2.1. Observations

We have made use of the *HST* Advanced Camera for Surveys using the Wide-Field Channel (ACS/WFC) (Program #13691, [Freedman 2014](#)), whose specifications and field selection criteria are described in [Paper I](#). In short, these include placement along galaxies’ minor axes to maximize the number of halo stars while avoiding disks and tidal structures. [Figure 1](#) displays the imaging coverage for this study, and [Table 1](#) provides a summary of the observations.

Observations were taken mid-2015 over a span of 8-9 days for each galaxy. For NGC 1448, 4 and 8 orbits were devoted to imaging in the F606W and F814W filters, respectively; for NGC 1316, 6 and 10 orbits were devoted to the respective filters. Exposure durations of ~ 1200 sec for each filter were set in order to achieve a signal-to-noise of 10 at the anticipated magnitude of the TRGB. The images used in the analysis are the FLC type, which are calibrated, flat-fielded, and CTE-corrected. We further corrected the images by multiply-

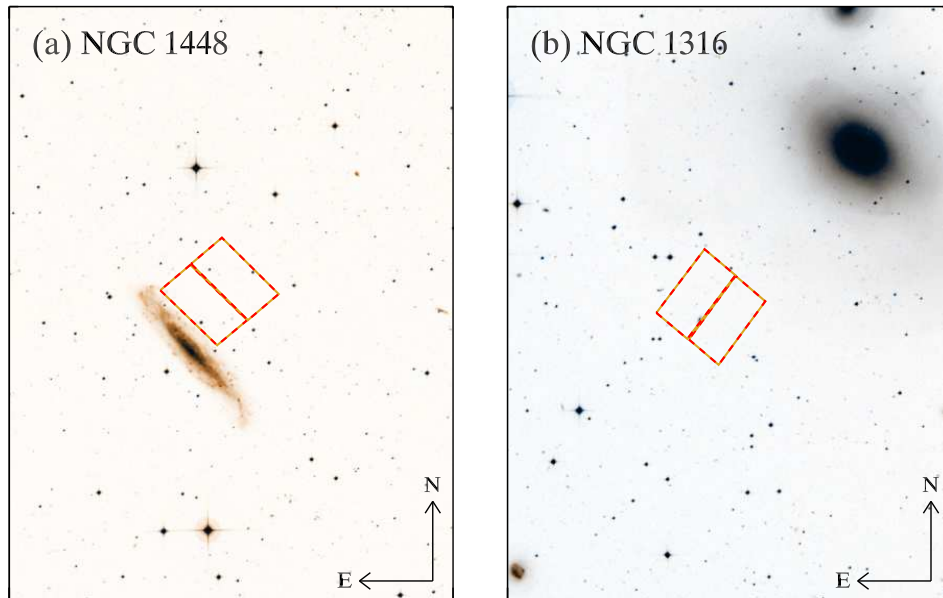


Figure 1. Locations of $3'37 \times 3'37$ *HST* ACS/WFC imaging (boxes) overlaid on an inverted color DSS image for (a) NGC 1448 and (b) NGC 1316.

Table 1. ACS/WFC Observation Summary

Target	Dates	Filters [No. obs \times exptime (s)]	α (2000)	δ (2000)	Field Size
NGC 1448	2015 Apr 03-12	F606W [7 \times 1200], F814W [15 \times 1200]	$03^h 44^m 27^s$	$-44^\circ 36' 14''$	$3'37 \times 3'37$
NGC 1316	2015 Jul 03-11	F606W [12 \times 1200], F814W [20 \times 1200]	$03^h 23^m 13^s$	$-37^\circ 19' 22''$	$3'37 \times 3'37$

NOTE—See also Figure 1 for imaging coverage.

ing by their Pixel Area Maps¹ to account for geometric distortions in the ACS/WFC camera.

2.2. Photometry

Photometry was performed identically to that described in Section 2 of Paper II and Paper III. In brief, photometry was carried out using the DAOPHOT suite of software (Stetson 1987) using Point-Spread-Functions (PSFs) that were obtained through the *HST* Tiny Tim PSF modeling software (Krist et al. 2011). Instrumental photometry was filtered for point sources through simple magnitude error and DAOPHOT ‘chi’ and ‘sharpness’ cuts: $F814W_{\text{err}} < 0.015 + 0.003 \cdot \exp(F814W - 23.75)$, $\text{chi} < 1.8$, and $-0.3 < \text{sharp} < 0.2$.

The calibration of instrumental magnitudes to the Vegamag system then followed the prescription in Sirianni et al. (2005). We refer the reader to the detailed assessment of possible systematic uncertainties in the calibration process in Section 2 of Paper III, which include considerations of the uncertainty in Encircled-Energies for a given aperture size and in the flux of Vega itself. The photometric zero-points used in the following analysis, subject to change at future dates via the online calculator², are 26.405 mag for F606W and 25.517 mag for F814W, accessed on 2018-06-11. While calibration constants like the photometric zero-points are largely unchanged between the works in the CCHF because they belong to a single *HST* observing cycle,

¹ <http://www.stsci.edu/hst/acs/analysis/PAMS>

² <https://acszeropoints.stsci.edu/>

Table 2. Average measured aperture corrections at $0''.5$

Target	CCD1		CCD2	
	F606W (No.)	F814W (No.)	F606W (No.)	F814W (No.)
NGC 1448	-0.16(14)	-0.14(33)	-0.13(8)	-0.12(33)
NGC 1316	-0.13(15)	-0.09(24)	-0.13(26)	-0.08(50)

NOTE—Parentheses are the total number of bright, isolated stars used in computing the average aperture corrections. Approximately equal numbers of stars are available in each image for aperture corrections on a frame-by-frame basis.

unique here are the measured aperture corrections at $0''.5$ whose averages we list in Table 2. In practice, these aperture corrections vary between exposures for a given filter at the 0.03-0.05 mag level. As per Sirianni et al. (2005), they are applied in the following analysis on a frame-by-frame basis, but we have found in the previous papers in this series, as well as in the current work, that the TRGB science result is unchanged to within the reported uncertainties if using only the average.

2.3. Color-magnitude diagrams

The calibrated photometry is presented in the form of CMDs in Figure 2. Error bars show sample median color and magnitude uncertainties. Each CMD shows a dominant halo component, i.e. an RGB, mixed with likely Thermally-Pulsating Asymptotic Giant Branch (TP-AGB) stars as well as early-type AGB (E-AGB) stars. Hereafter, we often refer to the two AGB classes as a single ‘AGB’ component that spans the full magnitude range of the RGB and extends brighter than the tip of the RGB. In Sections 3.2–3.3, we address the possibility of contamination in our measurement of the TRGB by AGB sources as well as assess the level of photometric completeness and crowding/blending through extensive artificial star tests. In addition to an RGB/AGB component, each CMD contains a muted blue component centered near $F606W - F814W = 0.0$. These objects are possibly young and massive stars, but they also occupy a color-magnitude space populated by components of background galaxies that pass photometry selection criteria. In either case, we explore the use of a color-magnitude selection cut to further isolate the RGB/TRGB in Section 3.5.

Each CMD contains a large enough sample of stars such that the RGB is well-populated. Madore et al. (2009) showed that ~ 400 stars were needed in the first magnitude below the TRGB to achieve ± 0.1 mag preci-

sion in the measurement of the TRGB. For these galaxies, the counts are over an order of magnitude larger, suggesting that the statistical (random) uncertainty in the TRGB measurement will be small. We note, however, that compared to higher signal-to-noise CMDs like that of IC 1613 in Paper II, the TRGB for each galaxy may be not as visually sharp due to larger photometric uncertainties. Then, in the case of distant galaxies such as those presented here, a precise measure of the TRGB magnitude is made possible through large population counts rather than a small number of well-measured, individual stars.

3. THE TIP OF THE RED GIANT BRANCH

3.1. Background

The TRGB is marked by a jump in a galaxy’s luminosity function between the foreground/AGB populations and the RGB. In the I -band (or more specifically its *HST* equivalent, F814W), the observed TRGB is remarkably fixed in brightness for observations of metal-poor stars, such as the galaxy halo imaging presented here. Note also that color-magnitude corrections for higher-metallicity stars have recently been calibrated empirically for ACS/WFC filters by (Jang & Lee 2017). In the case of such halo observations, where only AGB and RGB components are expected, it follows that the location of the TRGB is defined by the point of greatest change in the one-dimensional transition in star count (as a function of magnitude) between the two populations.

The simplicity of the TRGB method in the I -band allows for the application of basic yet robust tools to measure this point of transition. An overview of the CCHP approach to the TRGB method, as well as comparisons to existing methods, are given in Paper II and Paper III. In brief, an edge-detector measures the first-derivative of finely binned and smoothed foreground/AGB and

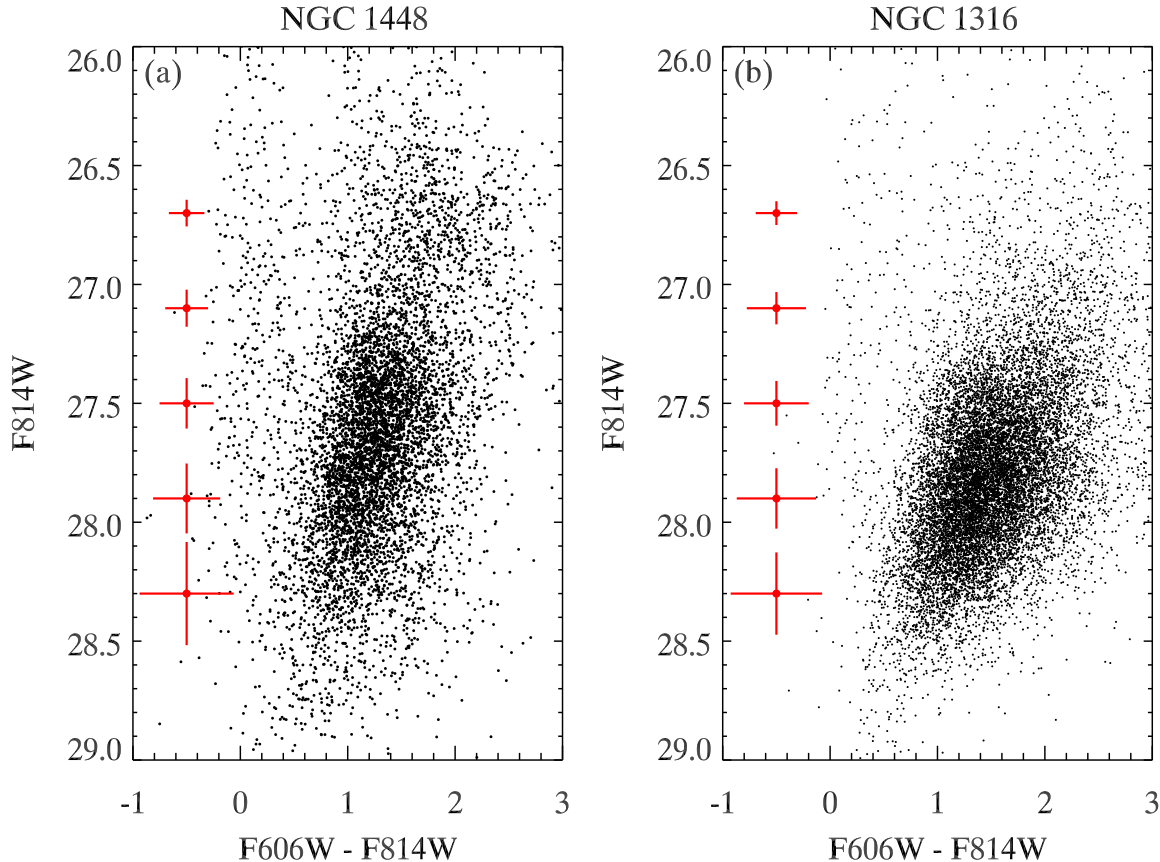


Figure 2. Color-magnitude diagrams of the galaxies NGC 1448 and NGC 1316. Likely TP-AGB stars are visible above the Red Giant Branch, although an abrupt jump in the luminosity function of each CMD, shown later in Section 3.5, still clearly marks the location of the TRGB. Median magnitude and color error bars are plotted alongside the CMDs.

AGB/RGB luminosity functions, $[-1, 0, +1]$, and returns a maximum response at the location of the TRGB. A common alternate method to measuring the TRGB is the simultaneous fit of the slopes of the AGB and RGB luminosity functions via a Maximum Likelihood estimator (often cited is Makarov et al. 2006). In the appendices of Hatt et al. (2017) and Jang et al. (2018), we compare the performance of the most common edge-detection methods for galaxies IC 1613 and NGC 1365 and find no statistically significant difference in their measured TRGB values. Since IC 1613 and NGC 1365 represent some of the nearest and furthest galaxies in the CCHP sample, the equal performance of the edge-detection methods suggests that the edge-detection methodology applied here is suitable for all other CCHP galaxy targets as well.

In the following sub-sections, we describe how the parameters for the smoothing of the data are chosen in order to optimize the measurement of the TRGB for each galaxy.

3.2. Artificial stars and luminosity functions

We generate artificial AGB and RGB star populations, consistent with the previous papers in this series, in order to model the observed luminosity function around the TRGB as closely as possible. We adopt AGB and RGB population slopes of 0.1 dex and 0.3 dex, respectively. The RGB luminosity function begins at the input TRGB value and extends 1 magnitude fainter. The input TRGBs have been adjusted for the galaxies at hand, which we have set to the approximate and preliminary TRGB measurements of 27.3 mag and 27.5 mag for NGC 1448 and NGC 1316, respectively. The AGB luminosity function begins 1 mag brighter than the input TRGB and extends the entire range of the RGB luminosity function. The relative counts of RGB:AGB stars is set to 4:1 at the TRGB to be consistent with recently observed population statistics in local galaxies (see e.g. Rosenfield et al. 2014, among others). Stars were randomly assigned colors from a uniform distribution between $1.0 \leq F606W - F814W \leq 1.5$ to model the approximate widths of the observed CMDs. For a given iteration, 2000 stars are sampled from these distributions and placed into each CCD. Photometry is performed

identically to before, and the measured magnitudes are recorded. The process of generating and measuring artificial stars is repeated 250 times for each CCD, resulting in a cumulative 500,000 simulated stars for each galaxy. The input and measured (output) luminosity functions for each galaxy are shown in [Figure 3a](#).

3.3. Photometric completeness and crowding

The large number of artificial stars allows us to assess the quality of our photometry, including completeness (fraction of recovered input stars) as well as accuracy. As with the other galaxies in the [CCHP](#) series, we find high completeness in F814W. Specifically, we find $\sim 90\%$ completeness at 0.5 mag below (fainter than) the TRGB and $\sim 80\%$ completeness 1 mag below the TRGB. We also find that there is no significant average deviation from the input magnitude near the TRGB. In other words, although the scatter of measured magnitudes increases with magnitude due to deterioration in signal-to-noise, there is no significant systematic offset at the magnitude range in question.

Beyond the median difference between input and output magnitudes from artificial stars, it is still possible to have blends, which, being shifted systematically brighter, could obscure the TRGB. We evaluated the possibility of blends following the surface brightness arguments in [Renzini \(1998\)](#). In [Paper IV](#), it was found that only the $\sim 10\%$ of the NGC 4424 footprint closest to the galaxy had a likelihood of $> 5\%$ of containing blends of RGB and AGB populations. In both NGC 1448 and NGC 1316, the surface brightnesses are lower (lower surface density of sources) resulting in the probability of blends being negligible ($\ll 1\%$).

3.4. Optimizing the TRGB edge detection

We now investigate how a randomly generated subset of our artificial star luminosity functions—comparable in count to the observed luminosity functions—affects the measurement of the TRGB as a function of the smoothing in the binned luminosity function. For this and previous works in the [CCHP](#) series, our smoothing function is GLOESS (Gaussian-windowed, Locally-Weighted Scatterplot Smoothing), which is a non-parametric interpolation technique. For a single iteration, the luminosity function subset of stars is binned, smoothed, and measured with our edge-detector identically to that of the real dataset. For each simulated TRGB detection, we record its location and the level of smoothing, which we label σ_s . Ten-thousand TRGB simulations were carried out for each smoothing scale in the range of 0.01-0.18 mag in 0.01 mag intervals.

The results of these simulations are given in panels (b) and (c) of [Figure 3](#). Panel (b) displays the depen-

dency of the average measured location of the TRGB, $\Delta\mu_{\text{TRGB}}$, and the dispersion of measurements, σ_{TRGB} , on the level of smoothing of the luminosity function. Panel (c) displays the dispersion of measured TRGB values from the simulations for the chosen “optimal” level of smoothing.

NGC 1448 and NGC 1316 display well-behaved dependencies on smoothing: under-smoothing the luminosity function results in triggering off noise but large levels of smoothing appear to have minimal impact on displacing the location of the input TRGB (low systematic error). For NGC 1448, we have chosen a value of $\sigma_s = 0.12$ mag to minimize the statistical uncertainty associated with the measurement while being cautious not to over-smooth the data, which in cases of less-idealized datasets could cause competing peaks in the edge-detector to merge, resulting in a robust but displaced (systematically offset) TRGB measurement. The predicted systematic uncertainty for the chosen level of smoothing is a negligible < 0.01 mag, and at this level, the width of the distribution of measured TRGBs (the statistical uncertainty) is ~ 0.02 mag (see [Figure 3c](#)).

In the case of NGC 1316, we have chosen a smaller smoothing scale of $\sigma_s = 0.05$ mag because of competing edge detections in the real dataset ~ 0.2 – 0.3 mag fainter within the RGB luminosity function. We revisit this observation later in [Sections 3.5](#) and [4.2](#) and discuss its possible origin. The smoothing scale chosen here is therefore intended to be small enough to resolve the peaks in the edge-detector while being large enough to suppress the likelihood of a false positive in the TRGB detection. The anticipated systematic effect on the TRGB measurement is ~ 0.01 mag while the statistical uncertainty is estimated to be ~ 0.03 mag.

Since AGB stars only blur the TRGB edge-detection, fewer AGB stars than the RGB:AGB ratio assumed here will only decrease the expected measurement uncertainty. To test for an extreme abundance of AGB stars, we decreased the ratio of RGB:AGB to 1:1 (a population at the TRGB that is 50% AGB), then re-ran our TRGB edge-detection simulations for NGC 1316 as a test case. We found that the systematic uncertainty increased to only ~ 0.02 mag from virtually no systematic effect. This result suggests that the S/N of the TRGB discontinuity is sufficiently large to retain high measurement precision even in a ‘worst-case’ scenario of RGB:AGB population abundances.

3.5. TRGB Measurements and Distances

In order to isolate the RGB and achieve the most accurate measurement of the TRGB, we have tested the effect of a color-magnitude selection filter to remove any

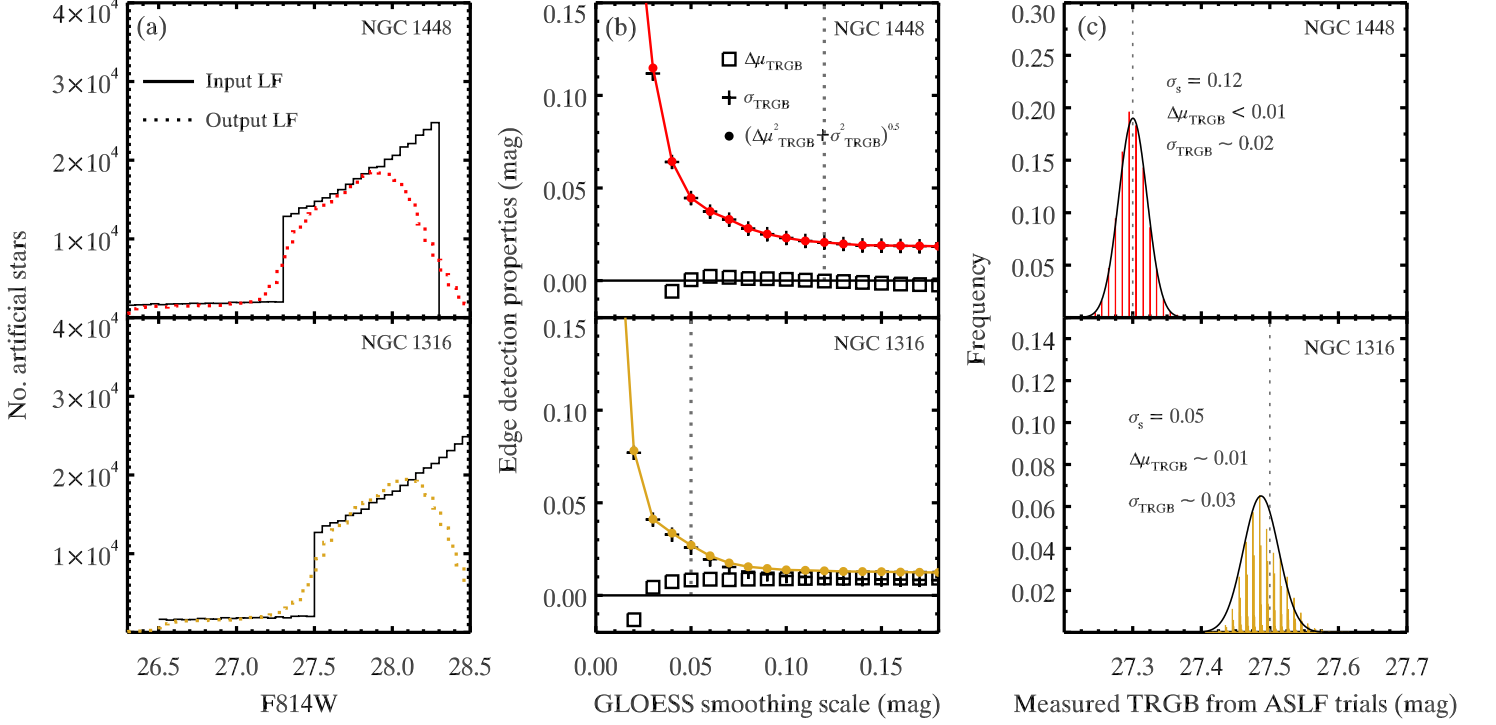


Figure 3. Estimating edge detection uncertainties through artificial star tests. Left Panel (a) input (solid) and output (dashed) AGB+RGB artificial star luminosity functions. The input TRGBs for NGC 1448 and NGC 1316 27.3 mag and 27.5 mag, respectively. Middle Panel (b) Statistical/random (plus signs), systematic (squares), and combined measurement uncertainties (points and lines) associated with the $[-1, 0, +1]$ Sobel edge-detection kernel as a function of GLOESS smoothing scale for each galaxy. Dotted vertical lines mark the chosen level of smoothing for each galaxy. Right Panel (c) The distribution of measured TRGB values at the optimal/chosen level of GLOESS smoothing.

Table 3. Summary of TRGB distances to NGC 1448 and NGC 1316

Galaxy	m_{TRGB}^a	σ_m^b	A_{F814W}	$(m - M)_0^c$	σ_{stat}	σ_{sys}	D (Mpc)	σ_{stat}	σ_{sys}
NGC 1448	27.26	0.04	0.02	31.23	0.04	0.06	17.7	0.3	0.5
NGC 1316	27.40	0.04	0.03	31.37	0.04	0.06	18.8	0.3	0.5

NOTE—Uncertainties in the above distance moduli and physical distances are dominated by the TRGB zero-point and are comparable at the ± 0.01 mag level of precision.

^aF814W

^bCombined statistical and systematic uncertainties from the edge detection method and calibration to the *HST* flight magnitude system.

^c $M_I^{\text{TRGB}} = -4.00 \pm 0.03 \pm 0.05$ mag

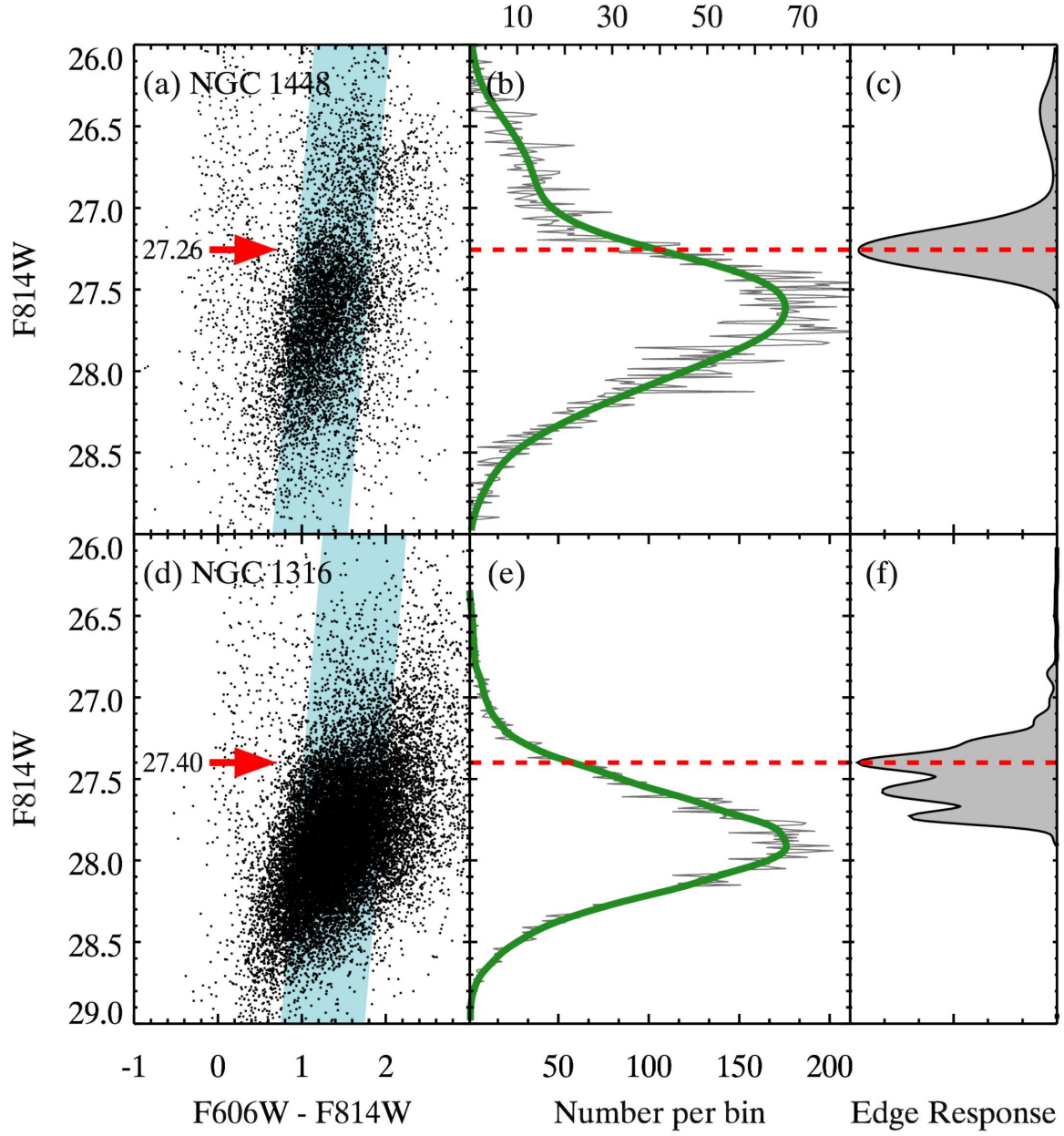


Figure 4. TRGB edge detection for NGC1448 and NGC1316. Panels (a) and (d) display the CMDs. A red arrow in each plot shows the location of the measured TRGB. Panels (b) and (e) show the binned luminosity functions in 0.01 mag intervals in gray and the GLOESS-smoothed luminosity functions in solid green. Panels (c) and (f) show the response function of the $[-1, 0, +1]$ kernel on the smoothed luminosity functions. These functions are scaled so that their peaks align. A dashed line passes through the location of the greatest change in the luminosity functions.

possible contamination by blue sources that are distinct from the AGB/RGB sequences. The slope of the selection windows, -6 mag/color , are measured from CCHP ACS/WFC observations of the high S/N and high completeness RGB of M31. The left edge of the windows are set to visually rest against the blue edges of the RGB, and we set the red edge of the window to visually encompass the RGB up to $F606W - F814W = 2.0$, which is the likely maximum extent of metal-poor stars based on the color uncertainties. At the chosen levels of GLOESS smoothing, we find that the value of the TRGB does not differ by more than 0.01 mag from that with no color-magnitude filter. Nevertheless, we apply the color-magnitude selection window for our measurements in the following to ensure any possible systematics are minimized.

The targets of this study were chosen, in part, because of their estimated low foreground extinction (i.e., $E(B - V) \leq 0.02$ (Schlafly & Finkbeiner 2011, obtained via NED). Adopting a Cardelli et al. (1989) reddening law, the predicted foreground reddening values are $A_{F814W} = 0.02 \text{ mag}$ and $A_{F814W} = 0.03 \text{ mag}$ for NGC 1448 and NGC 1316, respectively. The uncertainty in $E(B - V)$ is estimated to be $\pm 0.03 \text{ mag}$ (Schlegel et al. 1998), which suggests that the foreground extinction for each of these galaxies are statistically consistent with zero. We conservatively include half of the value of the estimated reddening as an additional systematic error in the distance moduli derived below.

Although the foreground reddening is predicted to be very low, it is not yet possible to assess whether there is extinction intrinsic to the halos themselves. One possible test for the presence of halo dust, however, is to observe whether or not the apparent TRGB magnitude changes with increasing distance into the halo. We tested this possibility by dividing the images into two distinct regions having equal numbers of stars. We reran our TRGB simulations with the adjusted star counts for this new test to find the appropriate level of GLOESS smoothing to minimize the combined measurement uncertainties. We found that even with the reduced statistics, the required level of smoothing is comparable to its original value that was found for the full catalogs. In the case of NGC 1448, the measured TRGB for the region closest to the galaxy agreed with the further region to within 0.01 mag. For NGC 1448, we thus conclude that there is insufficient evidence for halo dust within the current observation footprint.

In the case of possible halo reddening for NGC 1316, the difference in measured TRGB widens to $\sim 0.2 \text{ mag}$, where secondary peaks from the edge-detector (described in Section 3.4) become the dominant signals.

This difference could suggest the existence of halo reddening, but by further dividing the imaging into quarters, for example, it is apparent that the measured TRGB values are not a function of radial distance from the galaxy. Instead, the stars contributing to the peaks are spread approximately equally across the entire footprint, and the shift in dominance between the edge detection peaks appears to be due to fluctuations in population counts. In Section 4.2, we discuss the possible origin of the additional peaks within the RGB. Since the additional peaks appear to lie firmly within the RGB itself, we associate only the first (and most prominent peak with the full dataset) with the TRGB. In the measurement of NGC 1316 TRGB below, we note that we exclude a small region occupied by a recently discovered dwarf galaxy, Fornax UFD1, belonging to NGC 1316 (Lee et al. 2017), which covers only 0.07% of the footprint.

We turn now to the question of metallicity. At high metallicity, a downward sloping TRGB is observed in color-magnitude space for the reddest stars at optical wavelengths, although this effect is greatly diminished in the I -band/F814W. In addition, the observations used in this study were specifically crafted to target the metal-poor halos of these galaxies. As a result, given that the TRGBs in our sample of galaxy halos do not show any discernible color-magnitude dependence, we do not apply color-magnitude “rectification” tools (for ACS filters see Jang & Lee 2017).

Figure 4 displays the results of the TRGB measurement using the optimally selected GLOESS-smoothing scales for each galaxy. We find the following F814W (I -band equivalent) TRGB magnitudes: for NGC 1448, $I(\text{TRGB}) = 27.26 \pm 0.04 \text{ mag}$, and for NGC 1316, $I(\text{TRGB}) = 27.40 \pm 0.04 \text{ mag}$. These uncertainties combine both the statistical and systematic associated with the calibration and measurement. As with previous papers in this series, we adopt a provisional zero-point for the I -band/F814W TRGB based on the geometric distance to the Large Magellanic Cloud and an average of published I -band TRGB magnitudes in the literature. Adopting $E(B - V) = 0.03 \pm 0.03 \text{ mag}$ for the reddening of the LMC TRGB stars (see Hoyt et al. 2018), we derive $M_I = -4.00 \text{ mag} \pm 0.03_{\text{stat}} \pm 0.05_{\text{sys}}$. A summary of the TRGB measurements and extinction-corrected distances is given in Table 3. In the following section, we compare our findings with previously determined estimates.

In the previous section, we derived measurement uncertainty estimates for anticipated TRGB values of 27.3 and 27.5 mag for NGC 1448 and NGC 1316, respectively, which we note are not identical to those mea-

sured with the real datasets. The major driving factor in how well the TRGB is measured for a given amount of data smoothing is the typical photometric uncertainties of stars at the TRGB interface. Since the spread in photometric uncertainties for stars near the anticipated TRGBs is greater than the difference between our simulated and measured TRGB values, we expect no significant change in the estimated TRGB measurement uncertainty should we have generated new artificial stars and simulations.

4. DISTANCE COMPARISONS

4.1. *NGC 1448*

Distance estimates for NGC 1448 are based primarily on Tully-Fisher, SN Ia or SNe II. There are 2 ‘modern’ (since the year 2000) publications at the time of writing for the Tully-Fisher method (Springob et al. 2009; Tully et al. 2016), and we have used the publications that make use of the most current observations that are part of surveys. The Tully-Fisher relation produces an average distance modulus of 31.35 ± 0.12 mag. We have taken these published distances at face value and have not adjusted in any way for their assumptions on zero-point, extinction, etc. The Tully-Fisher method is in good agreement with our distance modulus of $31.23 \pm 0.04_{stat} \pm 0.06_{sys}$ mag (1 standard deviation of the average error in distance).

Regarding the supernovae distances, a direct comparison is not entirely suitable here given the SN Ia calibration objectives of the CCHP. Nonetheless, we report their average distance since they are a considerable component of the literature for distances to NGC 1448. Among several publications, there is 1 publication with unique observations of the SN Ia (Krisciunas et al. 2003), which gives an *H*-band distance modulus of 31.04 ± 0.14 mag and a *BVI* distance of 31.29 ± 0.08 mag. The *H*-band distance appears to be only in approximate agreement ($\sim 2\text{-}\sigma$ of their reported uncertainties), but the optical distance is in good agreement with our TRGB distance to within the mutual reported errors.

Finally, a single Cepheid-based distance exists for NGC 1448. Riess et al. (2016b) quote an ‘‘approximate’’ Cepheid distance of 31.31 ± 0.05 mag. This distance is in agreement with ours to within $1.4\text{-}\sigma$ of their reported uncertainties, and our measurement is in agreement with theirs to within $1\text{-}\sigma$.

4.2. *NGC 1316*

The variety of distance determinations that exist for NGC 1316 include Tully-Fisher, Faber-Jackson, Surface Brightness Fluctuations (SBFs), Planetary Nebula Luminosity functions (PNLFs), Globular Cluster Lumi-

nosity Functions (GCLFs), and Cepheids, among others. The numerous methods that derive distances for NGC 1316 are largely or exclusively derived for the Fornax Cluster, however, not NGC 1316 itself, and are therefore not ideal for a comparison here against our direct measurement of the galaxy.

We have endeavored to select only those distances that pertain exclusively to NGC 1316. Regarding GCLFs, attempts have either resulted in poor fits (Villegas et al. 2010) or have been excluded from analysis because of peculiarities in their size distributions (Masters et al. 2010). Modern estimates from PNLFs, on the other hand, yield a distance modulus of $31.26^{+0.9}_{-0.12}$ mag (Feldmeier et al. 2007), which based on their estimated errors is only approximately $1\text{-}\sigma$ from our measurement. Next, SBFs produce an average distance modulus of 31.61 ± 0.04 mag (Tonry et al. 2001; Ajhar et al. 2001; Jensen et al. 2003; Cantiello et al. 2007; Blakeslee et al. 2009, 2010; Cantiello et al. 2013), where the median distance and median uncertainty for multiple measurements in a single publication are taken as representative.

The average distance from SBFs is ~ 0.2 mag fainter than our reported distance modulus, which is a substantial difference, but this average distance *is* curiously more closely associated with one of the distances that one of the secondary peaks in the edge-detector would yield, $\sim 31.6 - 31.7$ mag, under the assumption that it represents a TRGB measurement. This alignment is perhaps not a coincidence and suggests that different underlying populations along the line-of-sight of NGC 1316 could be affecting accurate measurements with SBFs where the populations cannot be distinguished, unlike this work where the populations can be distinguished using a CMD. To add weight to the argument of a distinct underlying population, either within NGC 1316 or along its line-of-sight, the greater distance from SBFs closely aligns with the average distance to the Fornax Cluster via, for example, Cepheids (31.60 ± 0.04 mag, Ferrarese et al. 2000). Although NGC 1316 is at the relative edge of the Cluster, it is bordered by several members that could have played a role in its merger history and may possibly contribute to the stellar populations along the line-of-sight. Furthermore, evidence of additional stellar populations within NGC 1316, possibly from merger events, have been suggested in recent articles (e.g. the presence of young globular clusters and field stars by Sesto et al. 2018).

The third direct distance measurement to NGC 1316 (i.e., not relying on the Fornax Cluster as a whole) is through its SN Ia. Though not an ideal comparison because of the SN Ia calibration goals of the CCHP, we include a discussion here for a broader reference point

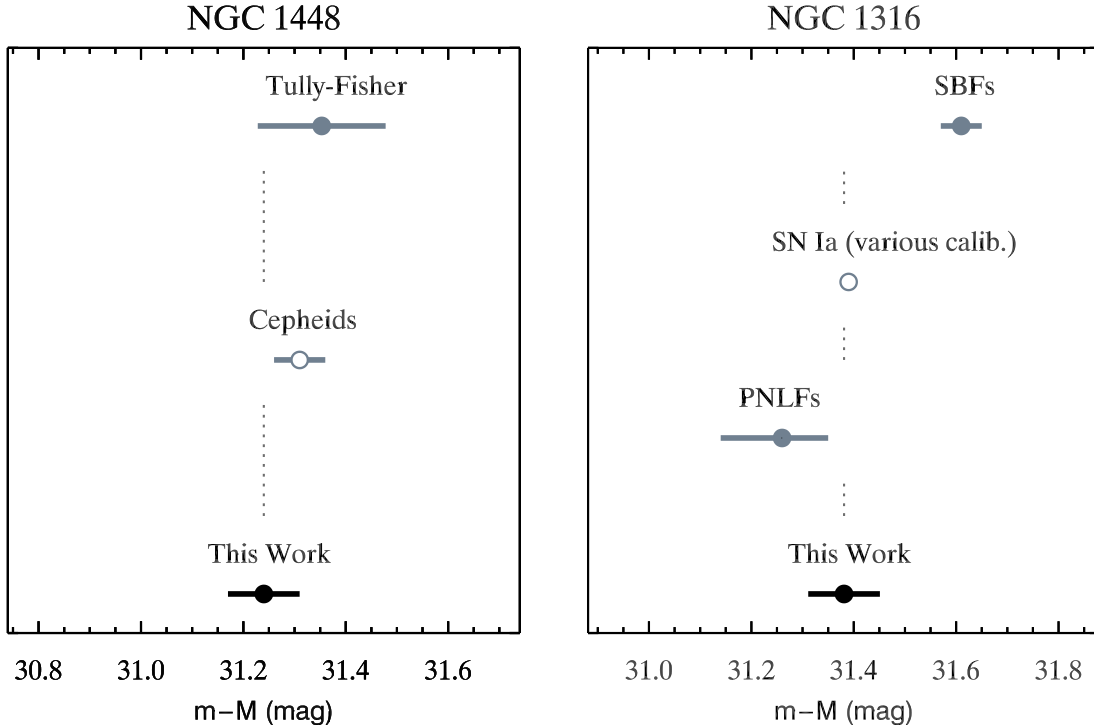


Figure 5. Distance moduli and their uncertainties as part of this work compared with the existing literature (statistical and systematic errors are added in quadrature). The Cepheid distance (only available for NGC 1448) is published as “approximate” and is denoted here by an open circle (see Table 5 of Riess et al. 2016a). SBFs, PNLFs, and the SN Ia of NGC 1316 are the only direct and reliable distance determinations to the galaxy (others report distances to the Fornax Cluster as a proxy). The SN Ia average is not an optimal comparative tool for our measurement given the calibration goals of the CCHP, but their average is presented here as a reference point (also denoted by an open circle) to compare against the large difference with SBFs. All measurements from the literature are taken at face value (non-adjusted for zero-points, extinction, etc.) and the displayed uncertainties are their respective errors on the mean. Vertical dotted lines pass through the results of this work.

to our measurement. The SNe Ia for NGC 1316 produce an average distance modulus of 31.39 ± 0.01 mag (the most comprehensive review having been done by Stritzinger et al. 2010), and our distance of $31.37 \pm 0.04_{stat} \pm 0.06_{sys}$ mag agrees to within a single standard deviation. The good agreement with the SN Ia distances, whose calibration is set by other methods and galaxies (often Cepheids), is reassuring in light of the large difference with SBFs.

Finally, the fourth distance to NGC 1316 comes from the recently discovered dwarf galaxy Fornax UFD1, also using the observations that are analyzed in this work. Its TRGB distance was measured to be 31.35 ± 0.15 mag (Lee et al. 2017), where we have adjusted their value for M_I (quoted in Jang & Lee 2017) to ours. The relatively small number of stars contributing to its TRGB inflates the uncertainty in its distance, but there is mutual agreement between the distances to within $1\text{-}\sigma$ of the quoted errors.

5. CONCLUSIONS

We have determined the first Tip of the Red Giant Branch distances for two SN Ia-host galaxies, NGC 1448 and NGC 1316, which are an integral part of an on-going effort by the CCHP to independently establish the SN Ia distance scale using Population II stars.

We find good agreement between these latest (and systematically independent) results in comparison to a variety of previously published distances for each of these galaxies. Moreover, the TRGB distances determined here are higher-precision than most existing estimates. Of publications that report smaller uncertainties in distance, most are derived from the SN Ia themselves that are inherently linked to a zero-point with an indeterminate or unreported systematic uncertainty. For this reason, the results presented here will serve as valuable, independent calibrators for the SN Ia extragalactic distance scale for the foreseeable future.

With future *Gaia* data releases, the CCHP will be refining the TRGB distance scale locally using Milky Way

RGB stars, thereby improving the zero-point accuracy of the TRGB method as a whole and further improving upon the systematics of the distances estimates reported here. Longer-term, with the pending launch of *JWST*, the galaxies studied here will serve as nearby rungs on the ever-increasing distance scale being built upon the TRGB method.

ACKNOWLEDGMENTS

We thank Peter Stetson for a copy of DAOPHOT as well as his helpful engagement on its usage. Support for this work was provided by NASA through Hubble Fellowship grant #51386.01 awarded to R.L.B. by the Space Telescope Science Institute, which is operated by the Association of Universities for Research in Astronomy, Inc., for NASA, under contract NAS 5-26555. Au-

thors MGL and ISJ were supported by the National Research Foundation of Korea (NRF) grant funded by the Korea Government (MSIP) No. 2017R1A2B4004632. Support for program #13691 was provided by NASA through a grant from the Space Telescope Science Institute, which is operated by the Association of Universities for Research in Astronomy, Inc., under NASA contract NAS 5-26555. This research has made use of the NASA/IPAC Extragalactic Database (NED), which is operated by the Jet Propulsion Laboratory, California Institute of Technology, under contract with the National Aeronautics and Space Administration.

Facility: HST (ACS/WFC)

Software: DAOPHOT (Stetson 1987), ALLFRAME (Stetson 1994), TinyTim (Krist et al. 2011)

REFERENCES

- Ajhar, E. A., Tonry, J. L., Blakeslee, J. P., Riess, A. G., & Schmidt, B. P. 2001, *ApJ*, 559, 584
- Beaton, R. L., Freedman, W. L., Madore, B. F., et al. 2016, *ApJ*, 832, 210
- Blakeslee, J. P., Jordán, A., Mei, S., et al. 2009, *ApJ*, 694, 556
- Blakeslee, J. P., Cantiello, M., Mei, S., et al. 2010, *ApJ*, 724, 657
- Cantiello, M., Blakeslee, J., Raimondo, G., Brocato, E., & Capaccioli, M. 2007, *ApJ*, 668, 130
- Cantiello, M., Grado, A., Blakeslee, J. P., et al. 2013, *A&A*, 552, A106
- Cardelli, J. A., Clayton, G. C., & Mathis, J. S. 1989, *ApJ*, 345, 245
- Feldmeier, J. J., Jacoby, G. H., & Phillips, M. M. 2007, *ApJ*, 657, 76
- Ferrarese, L., Mould, J. R., Kennicutt, Jr., R. C., et al. 2000, *ApJ*, 529, 745
- Freedman, W. 2014, CHP-II: The Carnegie Hubble Program to Measure H_0 to 3% Using Population II, HST Proposal, ,
- Freedman, W. L., Madore, B. F., Scowcroft, V., et al. 2012, *ApJ*, 758, 24
- Hatt, D., Beaton, R. L., Freedman, W. L., et al. 2017, *ApJ*, 845, 146
- Hatt, D., Freedman, W. L., Madore, B. F., et al. 2018, *ApJ*, 861, 104
- Hoyt, T. J., Freedman, W. L., Madore, B. F., et al. 2018, ArXiv e-prints, arXiv:1803.01277
- Jang, I. S., & Lee, M. G. 2017, *ApJ*, 835, 28
- Jang, I. S., Hatt, D., Beaton, R. L., et al. 2018, *ApJ*, 852, 60
- Jensen, J. B., Tonry, J. L., Barris, B. J., et al. 2003, *ApJ*, 583, 712
- Klagyivik, P., Szabados, L., Szing, A., Leccia, S., & Mowlavi, N. 2013, *MNRAS*, 434, 2418
- Komatsu, E., Smith, K. M., Dunkley, J., et al. 2011, *ApJS*, 192, 18
- Krisciunas, K., Suntzeff, N. B., Candia, P., et al. 2003, *AJ*, 125, 166
- Krist, J. E., Hook, R. N., & Stoehr, F. 2011, in *Proc. SPIE*, Vol. 8127, Optical Modeling and Performance Predictions V, 81270J
- Lee, M. G., Jang, I. S., Beaton, R., et al. 2017, *ApJ*, 835, L27
- Madore, B. F., Mager, V., & Freedman, W. L. 2009, *ApJ*, 690, 389
- Mager, V. A., Madore, B. F., & Freedman, W. L. 2013, *ApJ*, 777, 79
- Makarov, D., Makarova, L., Rizzi, L., et al. 2006, *AJ*, 132, 2729
- Masters, K. L., Jordán, A., Côté, P., et al. 2010, *ApJ*, 715, 1419
- Mochejska, B. J., Macri, L. M., Sasselov, D. D., & Stanek, K. Z. 2004, in *Astronomical Society of the Pacific Conference Series*, Vol. 310, IAU Colloq. 193: Variable Stars in the Local Group, ed. D. W. Kurtz & K. R. Pollard, 41
- Monard, A. G., Bock, G., Wassilieff, A., & Biggs, J. 2001, *IAU Circ.*, 7720
- Monard, L. A. G. 2006, *Central Bureau Electronic Telegrams*, 553
- Phillips, M. M., Folatelli, G., Contreras, C., & Morrell, N. 2006, *Central Bureau Electronic Telegrams*, 729

- Planck Collaboration, Aghanim, N., Akrami, Y., et al. 2018, ArXiv e-prints, arXiv:1807.06209
- Renzini, A. 1998, *AJ*, 115, 2459
- Riess, A. G., Macri, L. M., Hoffmann, S. L., et al. 2016a, *ApJ*, 826, 56
- . 2016b, *ApJ*, 826, 56
- Riess, A. G., Casertano, S., Yuan, W., et al. 2018, ArXiv e-prints, arXiv:1804.10655
- Rosenfield, P., Marigo, P., Girardi, L., et al. 2014, *ApJ*, 790, 22
- Sakai, S., Ferrarese, L., Kennicutt, Jr., R. C., & Saha, A. 2004, *ApJ*, 608, 42
- Salaris, M., & Cassisi, S. 2005, *Evolution of Stars and Stellar Populations*, 1st edn. (Wiley)
- Schlafly, E. F., & Finkbeiner, D. P. 2011, *ApJ*, 737, 103
- Schlegel, D. J., Finkbeiner, D. P., & Davis, M. 1998, *ApJ*, 500, 525
- Sesto, L. A., Faifer, F. R., Smith Castelli, A. V., Forte, J. C., & Escudero, C. G. 2018, *MNRAS*, arXiv:1806.00316
- Sirianni, M., Jee, M. J., Benítez, N., et al. 2005, *PASP*, 117, 1049
- Springob, C. M., Masters, K. L., Haynes, M. P., Giovanelli, R., & Marinoni, C. 2009, *ApJS*, 182, 474
- Stetson, P. B. 1987, *PASP*, 99, 191
- . 1994, *PASP*, 106, 250
- Stritzinger, M., Burns, C. R., Phillips, M. M., et al. 2010, *AJ*, 140, 2036
- Tonry, J. L., Dressler, A., Blakeslee, J. P., et al. 2001, *èpspj*, 546, 681
- Tully, R. B., Courtois, H. M., & Sorce, J. G. 2016, *AJ*, 152, 50
- Vilardell, F., Jordi, C., & Ribas, I. 2007, *A&A*, 473, 847
- Villegas, D., Jordán, A., Peng, E. W., et al. 2010, *ApJ*, 717, 603